

# Record High Hydrogen Storage Capacity in the Metal–Organic Framework $\text{Ni}_2(m\text{-dobdc})$ at Near-Ambient Temperatures

Matthew T. Kapelewski,<sup>†,‡</sup> Tomče Runčevski,<sup>†,‡</sup> Jacob D. Tarver,<sup>⊥,§</sup> Henry Z. H. Jiang,<sup>†,‡</sup> Katherine E. Hurst,<sup>§</sup> Philip A. Parilla,<sup>||</sup> Anthony Ayala,<sup>⊥,¶</sup> Thomas Gennett,<sup>§,#</sup> Stephen A. FitzGerald,<sup>□,⊙</sup> Craig M. Brown,<sup>⊥,⊙</sup> and Jeffrey R. Long<sup>\*,†,‡,△,⊙</sup>

<sup>†</sup>Department of Chemistry, University of California, Berkeley, Berkeley, California 94720, United States

<sup>‡</sup>Materials Sciences Division, Lawrence Berkeley National Laboratory, Berkeley, California 94720, United States

<sup>⊥</sup>Center for Neutron Research, National Institute of Standards and Technology, Gaithersburg, Maryland 20899, United States

<sup>§</sup>Chemistry & Nanoscience Center, National Renewable Energy Laboratory, Golden, Colorado 80401, United States

<sup>||</sup>Materials Science Center, National Renewable Energy Laboratory, Golden, Colorado 80401, United States

<sup>¶</sup>Department of Chemistry, University of Maryland, College Park, Maryland 20742, United States

<sup>#</sup>Department of Chemistry, Colorado School of Mines, Golden, Colorado 80401, United States

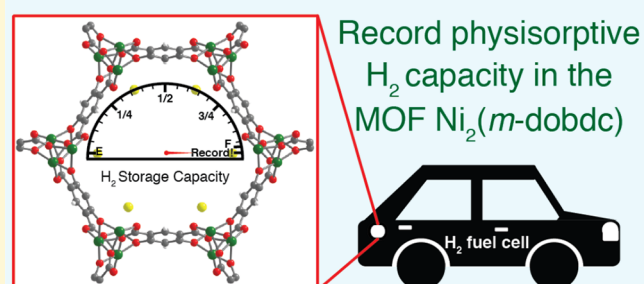
<sup>□</sup>Department of Physics, Oberlin College, Oberlin, Ohio 44074, United States

<sup>⊙</sup>Chemical and Biomolecular Engineering, University of Delaware, Newark, Delaware 19716, United States

<sup>△</sup>Department of Chemical and Biomolecular Engineering, University of California, Berkeley, Berkeley, California 94720, United States

## Supporting Information

**ABSTRACT:** Hydrogen holds promise as a clean alternative automobile fuel, but its on-board storage presents significant challenges due to the low temperatures and/or high pressures required to achieve a sufficient energy density. The opportunity to significantly reduce the required pressure for high density  $\text{H}_2$  storage persists for metal–organic frameworks due to their modular structures and large internal surface areas. The measurement of  $\text{H}_2$  adsorption in such materials under conditions most relevant to on-board storage is crucial to understanding how these materials would perform in actual applications, although such data have to date been lacking. In the present work, the metal–organic frameworks  $\text{M}_2(m\text{-dobdc})$  ( $\text{M} = \text{Co}, \text{Ni}$ ;  $m\text{-dobdc}^{4-} = 4,6\text{-dioxido-1,3-benzenedicarboxylate}$ ) and the isomeric frameworks  $\text{M}_2(\text{dobdc})$  ( $\text{M} = \text{Co}, \text{Ni}$ ;  $\text{dobdc}^{4-} = 1,4\text{-dioxido-1,3-benzenedicarboxylate}$ ), which are known to have open metal cation sites that strongly interact with  $\text{H}_2$ , were evaluated for their usable volumetric  $\text{H}_2$  storage capacities over a range of near-ambient temperatures relevant to on-board storage. Based upon adsorption isotherm data,  $\text{Ni}_2(m\text{-dobdc})$  was found to be the top-performing physisorptive storage material with a usable volumetric capacity between 100 and 5 bar of 11.0 g/L at 25 °C and 23.0 g/L with a temperature swing between −75 and 25 °C. Additional neutron diffraction and infrared spectroscopy experiments performed with *in situ* dosing of  $\text{D}_2$  or  $\text{H}_2$  were used to probe the hydrogen storage properties of these materials under the relevant conditions. The results provide benchmark characteristics for comparison with future attempts to achieve improved adsorbents for mobile hydrogen storage applications.



## INTRODUCTION

Molecular hydrogen ( $\text{H}_2$ ) holds significant promise as a transportation fuel and is already used in some motor vehicles and for certain specialty applications such as forklifts. Because water is the only byproduct of the fuel cell cycle, hydrogen fuel cell vehicles could, in principle, provide zero-emission transportation.<sup>1</sup> An economy can be envisioned in which solar energy is used to inexpensively produce hydrogen and oxygen from water; these products are then consumed in fuel

cells to produce water and electricity that power the vehicle and close the cycle. Achieving such an economy, however, requires the successful development of each aspect of this process to both efficiently produce  $\text{H}_2$  for use in fuel cells and consume  $\text{H}_2$  in the production of electricity.

Received: August 2, 2018

Revised: October 25, 2018

Significant investment in infrastructure supporting hydrogen fuel cell vehicles is underway around the world. As of 2017, the United States has 34 publicly accessible hydrogen fueling stations, with 31 of these in California.<sup>2</sup> The “California Hydrogen Highway” is a planned expansion of the current distribution network to 100 hydrogen fueling stations in California, primarily linking San Diego, Los Angeles, and the San Francisco Bay Area.<sup>3</sup> Other countries including Japan, France, Germany, and the United Kingdom have made significant investments in hydrogen infrastructure both in anticipation of and to help bring about the wider use of hydrogen fuel cell vehicles.<sup>4</sup> Public–private partnerships further these efforts and provide a basis for the future of hydrogen fuel cell vehicles to provide a clean alternative to traditional fossil-fuel-based transportation.<sup>5</sup> In addition to infrastructure developments, further scientific advances are imperative to realize the widespread adoption of hydrogen as a commercial fuel. Notable among such desired advances is the development of efficient hydrogen storage systems.<sup>6</sup> While containing 2.6–3 times more energy per unit mass than gasoline,<sup>7,8</sup> hydrogen poses challenges in the pursuit of storage at high volumetric densities. Hydrogen is a weakly interacting gas at ambient temperature and pressure and thus requires cooling and/or compression for storage at densities sufficient for acceptable driving ranges in automobiles. However, cryogenic storage requires the use of large, expensive, and well-insulated systems to maintain a low temperature.<sup>6,9</sup> Similarly, compression of H<sub>2</sub> at high pressures, typically up to 700 bar, is costly and requires heavy, expensive, and bulky storage tanks.<sup>10,11</sup> Both of these solutions therefore add to the price of the vehicle in addition to providing significant engineering challenges given the wide operating temperature range for passenger vehicles (−40 to 60 °C). Furthermore, compression to 700 bar results in a hydrogen volumetric energy density of only 5.6 MJ/L at 298 K, significantly lower than the 32.4 MJ/L for gasoline.<sup>8</sup> While the use of a metal or chemical hydride as a storage medium could mitigate the need for low temperature or high pressure storage vessels, these materials tend to suffer from either capacity limitations or problems arising from large activation energies and reversibility issues.<sup>12–15</sup>

An alternative to either cryogenic or compressive storage involves the use of an adsorbent material such as a zeolite<sup>16</sup> or activated carbon<sup>17</sup> to boost the hydrogen density in a tank under more ambient conditions. With just two electrons and a low polarizability, H<sub>2</sub> is capable of engaging in only weak van der Waals interactions, leading to an adsorption enthalpy that is typically on the order of −5 kJ/mol. Accordingly, adsorption sites capable of strongly polarizing H<sub>2</sub> must be introduced to achieve sufficient densification and a reasonable driving range. Cryo-adsorption, which entails a combination of adsorption and cryogenic storage, is one possible strategy to yield high capacities.<sup>18,19</sup> However, the ideal situation would involve adsorption under ambient temperature conditions with a relatively low fill pressure of 100 bar or lower. Such a system would be expected to lower costs significantly because a conformable, lightweight storage vessel could potentially be used, and no on-board cooling system would be required.

Metal–organic frameworks (MOFs) are a class of materials with great potential for hydrogen storage, among other applications related to gas storage and separations.<sup>20</sup> The inherent synthetic tunability of these structures has led to a wide range of interesting properties such as high surface

areas,<sup>21</sup> negative gas adsorption,<sup>22</sup> and precisely engineered pore environments.<sup>23</sup> Such tunability can be used to improve their properties for a desired application, including hydrogen storage,<sup>24–27</sup> and has made MOFs one of the most intensely studied fields in modern inorganic chemistry. For example, it is possible to create MOFs featuring pore surfaces with a high concentration of strong H<sub>2</sub> adsorption sites, a feature less readily achieved in zeolites and activated carbon adsorbents. Computationally predicted hydrogen adsorption isotherms in MOFs have shown high hydrogen capacities at near-ambient temperatures, but these materials have yet to be evaluated experimentally.<sup>28–31</sup> MOFs can thus, in principle, be designed to exhibit H<sub>2</sub> binding enthalpies in the optimal range of −15 to −20 kJ/mol,<sup>32</sup> leading to a high storage capacity under conditions relevant to light-duty fuel cell vehicles.<sup>33</sup> The appeal of this approach is apparent in the many studies of MOFs for H<sub>2</sub> storage that have often focused on materials containing coordinatively unsaturated (open) metal sites.<sup>34</sup> These exposed positive charges are able to polarize H<sub>2</sub> more strongly than the typical surfaces available for physisorption in most storage materials.<sup>35–38</sup> Thus far, however, no MOFs have been shown to achieve the necessary binding enthalpies or the capacity metrics set forth by the United States Department of Energy (US DOE).<sup>33</sup>

The most promising metal–organic framework identified to date for H<sub>2</sub> storage is Ni<sub>2</sub>(*m*-dobdc) (*m*-dobdc<sup>4−</sup> = 4,6-dioxido-1,3-benzenedicarboxylate), which was shown previously to display an H<sub>2</sub> binding enthalpy of −13.7 kJ/mol, as measured by variable-temperature infrared spectroscopy and representing the largest value yet observed in a MOF by this method.<sup>39</sup> Ni<sub>2</sub>(*m*-dobdc) is a structural isomer of Ni<sub>2</sub>(dobdc) (dobdc<sup>4−</sup> = 2,5-dioxido-1,4-benzenedicarboxylate; Ni-MOF-74), and its record binding enthalpy is largely a result of a higher charge density at its coordinatively unsaturated Ni<sup>2+</sup> centers. These sites strongly polarize H<sub>2</sub>, providing the primary binding sites for H<sub>2</sub> within the pores of the material and leading to a high gravimetric storage capacity of greater than 11 mmol/g (2.2 wt %) at 77 K and 1 bar. Recent reports have shown that the material Cu(I)-MFU-4l exhibits an H<sub>2</sub> isosteric heat of adsorption of −32 kJ/mol;<sup>40</sup> however, the volumetric density of these open metal coordination sites in this material is about 10% of that in Ni<sub>2</sub>(*m*-dobdc), rendering it perhaps more suitable for H<sub>2</sub>/D<sub>2</sub> separations than H<sub>2</sub> storage.<sup>41</sup>

In this work, we investigated the hydrogen storage properties of Ni<sub>2</sub>(*m*-dobdc) and other related top-performing MOFs, specifically Co<sub>2</sub>(*m*-dobdc), Co<sub>2</sub>(dobdc), and Ni<sub>2</sub>(dobdc), under more practical conditions. Adsorption isotherms at multiple temperatures in the range of 198 to 373 K were measured to determine capacities at pressure up to 100 bar, while *in situ* powder neutron diffraction and infrared spectroscopy experiments were employed to probe the nature of the interactions of hydrogen within the pores of the materials.

## ■ EXPERIMENTAL SECTION

**General Synthesis.** The compounds M<sub>2</sub>(*m*-dobdc) (M = Co, Ni) were synthesized and activated according to modified versions of the large-scale literature procedure.<sup>39</sup>

**Synthesis of H<sub>4</sub>(*m*-dobdc).** Resorcinol (1,3-dihydroxybenzene; 37.6 g, 0.341 mol) was pulverized and dried under vacuum. KHCO<sub>3</sub> (100 g, 0.99 mmol) was separately pulverized and dried under reduced pressure. The two powders were mixed together thoroughly and placed in a glass jar, which was sealed in a Parr reaction bomb equipped with an internal thermocouple and a pressure gauge. The

reaction bomb was evacuated under vacuum, and then CO<sub>2</sub> was dosed to a pressure of 40 bar. The bomb was heated to 250 °C (as measured by the internal thermocouple) in a sand bath for 24 h and then slowly cooled to room temperature. The pressure was vented; 1 L of water was added to the solid, which was broken up mechanically, and the mixture was sonicated. The resulting suspension was filtered, and the filtrate was acidified with 12 M HCl until a pH < 2 was achieved and a white solid had precipitated. This solid was collected by filtration and dried in air to yield 53.2 g (79%) of product. <sup>1</sup>H NMR (400 MHz, DMSO-*d*<sub>6</sub>) δ 9.22 (br, 4H), 8.28 (s, 1H), 6.22 (s, 1H); <sup>13</sup>C NMR (400 MHz, DMSO-*d*<sub>6</sub>) δ 172.0, 167.7, 134.3, 107.3, 103.0.

**Synthesis of Co<sub>2</sub>(*m*-dobdc).** Aliquots of 310 mL of methanol and 310 mL of *N,N*-dimethylformamide (DMF) were added to a 1-L three-neck round-bottom flask equipped with a reflux condenser and sparged with N<sub>2</sub> with stirring for 1 h. The solids H<sub>4</sub>(*m*-dobdc) (2.00 g, 10.1 mmol) and CoCl<sub>2</sub> (3.27 g, 25.2 mmol) were added under N<sub>2</sub> pressure, and the reaction mixture was vigorously stirred and heated at 120 °C for 18 h. The mixture was then cooled to ambient temperature and filtered, affording a pink microcrystalline powder. The powder was soaked in 500 mL of DMF for 24 h, then soaked in three successive aliquots of 500 mL of methanol for 24 h each. The resulting pink powder was collected by filtration and heated at 180 °C under dynamic vacuum until the outgas rate was <1 μbar/min, yielding 1.71 g (54.3%) of activated product.

**Synthesis of Ni<sub>2</sub>(*m*-dobdc).** An identical procedure was used as for Co<sub>2</sub>(*m*-dobdc) above, except that the solvent consisted of 220 mL of methanol and 405 mL DMF, and NiCl<sub>2</sub> (3.27 g, 25.2 mmol) was used in place of CoCl<sub>2</sub>. The reaction yielded 1.69 g (54.4%) of activated product.

**Synthesis of M<sub>2</sub>(dobdc) (M = Co, Ni).** These materials were synthesized using identical procedures to their M<sub>2</sub>(*m*-dobdc) congeners above, with the substitution of like amounts of the isomeric H<sub>4</sub>(dobdc) ligand for the H<sub>4</sub>(*m*-dobdc) ligand. These reactions yielded 2.06 g (65.4%) of activated Co<sub>2</sub>(dobdc) and 2.25 g (80.1%) of activated Ni<sub>2</sub>(dobdc).

**Synthesis of MOF-5.** The synthesis of MOF-5 was carried out according to a previously published procedure.<sup>42,43</sup>

**Measurement of Gas Adsorption Isotherms.** All gas adsorption isotherms in the range 198 to 373 K were measured on a Particulate Systems HPVA II instrument. The sample holder was custom-built using a Swagelok valve connected to a sample holder. Typically, 1.0–2.0 g of sample was used for each measurement to ensure that measurement and mass errors were minimized. These samples were activated in standard glass sample tubes as loose powders on a Micromeritics ASAP 2420 instrument and transferred to the custom HPVA sample holder in a drybox. Once the sample holder was connected to the HPVA instrument, the sample was immersed in a recirculating fluid bath connected to a Julabo FP89-HL/TK filled with Dow Syltherm fluid. During the data collection, a portion of the sample holder was exposed above the fluid in the temperature bath but below the temperature-controlled dosing manifold of the HPVA-II instrument. The resulting existence of three temperature zones leads to challenges in performing the required volume calibrations, which are essential to properly determining the gas uptake of a sample. The volume of each temperature zone was therefore experimentally determined based on He measurements at multiple temperatures, and the results were applied in obtaining corrected adsorption data. A more complete discussion of this calibration method can be found in a similar paper discussing the measurement of methane adsorption in MOFs.<sup>42</sup>

Importantly, the background adsorption of H<sub>2</sub> within the sample in an empty sample holder should be close to zero at all pressures, assuming the proper calibrations are in place. While this is true for isotherms being measured at close to ambient temperature (at which the temperatures of the two parts of the sample holder are very similar, resulting in a minimal temperature gradient), isotherms measured at temperatures further from ambient will see a larger temperature gradient and a commensurate deviation from null adsorption. To account for this deviation, background adsorption measurements for H<sub>2</sub> were repeated three times at each temperature

and fit using a third-order polynomial, which was then used to perform a background correction on all subsequently collected data at each temperature. The uptake in these background adsorption isotherms was typically on the order of 10 v/v (volume of H<sub>2</sub> per volume of MOF), and the measured values were subtracted from the total adsorption isotherms of the metal–organic frameworks. Such error primarily stems from minor temperature fluctuations in the three-zone experimental setup as well as small valve volumes. Pore volumes were determined experimentally using N<sub>2</sub> adsorption isotherm data. Pore volumes were determined to be 0.53, 0.56, 0.52, and 0.54 cm<sup>3</sup>/g for Co<sub>2</sub>(*m*-dobdc), Ni<sub>2</sub>(*m*-dobdc), Co<sub>2</sub>(dobdc), and Ni<sub>2</sub>(dobdc), respectively. Crystallographic densities were used in all calculations to obtain volumetric capacities.

Adsorption isotherms at 77 and 100 K (Figures S2 and S3) were collected on a custom-built volumetric adsorption apparatus at the National Renewable Energy Laboratory (NREL), details of which can be found in the Supporting Information.

**Temperature-Programmed Desorption.** The temperature-programmed desorption (TPD) data were collected on a custom-built NREL TPD apparatus that allows for identification and quantification of effluent gases, as described elsewhere.<sup>44</sup> In summary, calibrated adsorption capacities and desorption activation energies and kinetics can be investigated using the system, in which it is possible to heat or cool samples in vacuum to temperatures between 77 and 1200 K. Samples may be exposed to hydrogen (99.9999%) at pressures up to ~1000 Torr, and the system can achieve pressures as low as 10<sup>−9</sup> Torr. The TPD system is equipped with a mass spectrometer with detection range of 0–100 atomic mass units to detect impurities present in materials both during degas and after hydrogen exposures.

**Powder Neutron Diffraction Measurements.** Powder neutron diffraction data were collected on the high resolution neutron powder diffractometer, BT-1, at the National Institutes of Standards and Technology (NIST) Center for Neutron Research (NCNR), with a Ge-(311) monochromator using an in-pile 60' collimator corresponding to a wavelength of 2.077 Å. Measurements were performed on 1.11 g of activated Co<sub>2</sub>(*m*-dobdc). The activated sample was transferred into a He-purged glovebox equipped with oxygen and water monitors. The sample was loaded into an aluminum can equipped with a valve for gas loading up to pressures of 100 bar and loaded into a top-loading closed-cycle refrigerator. Data collection was performed at 77 and 198 K for the activated sample. At 77 K, one loading of 78 bar of D<sub>2</sub> was measured. At 198 K, the sample was initially exposed to 79 bar of D<sub>2</sub> and allowed to reach equilibrium. Additional measurements were performed at reduced pressures of 54 and 36 bar of D<sub>2</sub>. Aluminum Bragg peaks were removed from the data during analysis.

**In Situ Infrared Spectroscopy.** Infrared spectra were acquired using a Bomem DA3 Michelson interferometer equipped with a quartz-halogen source, a CaF<sub>2</sub> beamsplitter, and a liquid nitrogen-cooled mercury–cadmium–telluride detector. A cutoff filter above 9000 cm<sup>−1</sup> was used to prevent unwanted sample heating from the IR source. A custom-built diffuse reflectance system with a sample chamber that allows both the temperature and atmosphere of the material to be controlled was utilized for all experiments.<sup>45</sup> Activated powder samples (~10 mg) were transferred to a Cu sample holder within an Ar-purged glovebox. The samples were sealed within a dome containing sapphire windows and a valve for gas loading. Seals were achieved using either indium or Teflon gaskets depending on the pressure and temperature of the specific experiment. The dome was bolted to a copper slab providing thermal contact to a coldfinger cryostat (Janis ST-300T). The sample temperature was monitored by a Si-diode thermometer bolted directly to the copper slab. A reference infrared spectrum was obtained at each temperature. Hydrogen gas was introduced from a dosing manifold to a desired pressure while maintaining the sample at constant temperature. Multiple infrared spectra were obtained at each pressure step up to a maximum pressure of 100 bar. These spectra were then referenced to the initial spectrum without H<sub>2</sub>.



## RESULTS AND DISCUSSION

**General Considerations for H<sub>2</sub> Storage in Adsorbents.** As introduced earlier, adsorbent materials have the potential to store H<sub>2</sub> at reduced pressures and temperatures relative to cryogenic or high-pressure technologies and therefore offer a more energetically and financially promising solution. The US DOE has released guidelines for hydrogen storage in light-duty and specialty vehicles (e.g., passenger vehicles, forklifts, golf carts, and specialized airport vehicles, among others). A subset of the system-based targets associated with these guidelines and relevant to adsorbent-based storage is reproduced in Table 1.

**Table 1. Selected US DOE Targets for the Onboard Storage of Hydrogen in Light-Duty Fuel Cell Vehicles<sup>33</sup>**

storage parameter	units	2020	ultimate
system gravimetric H <sub>2</sub> capacity	kg H <sub>2</sub> /kg system, kWh/kg	0.045, 1.5	0.065, 2.2
system volumetric H <sub>2</sub> capacity	g H <sub>2</sub> /L system, kWh/L	30, 1.0	50, 1.7
storage system cost	\$/kg H <sub>2</sub> stored, \$/gge at pump	333, 4	266, 4
operating ambient temperature	°C	−40 to 60	−40 to 60
min/max delivery temperature	°C	−40 to 85	−40 to 85
operational cycle life (1/4 tank to full)	cycles	1500	1500
min delivery pressure from storage system	bar (abs)	5	5
max delivery pressure from storage system	bar (abs)	12	12
system fill time (5 kg)	min	3–5	3–5

To date, no adsorbents have been produced that satisfy the 2020 target capacity requirements of 4.5 wt % and 30 g/L H<sub>2</sub>. The trade-off between volumetric and gravimetric H<sub>2</sub> density in MOFs has been previously studied, however, showing maximization of both to be difficult.<sup>46,47</sup> While pressure ranges are not explicitly given, operating pressures below 100 bar have the potential to reduce storage vessel and compression costs while maintaining reasonable capacities. Importantly, these target capacity requirements are full system capacities. Therefore, potential adsorbent materials must actually exceed target capacities, as the full system will involve more mass and volume than that of the adsorbent alone.

The volumetric capacity is the primary consideration when evaluating MOF materials for H<sub>2</sub> storage, because in light-duty vehicles, the available volume for a tank for adsorbent-based storage of H<sub>2</sub> is the limiting factor in determining the driving range of a vehicle. This concept has been discussed in detail elsewhere for natural gas storage,<sup>42</sup> and the same principles will apply to H<sub>2</sub> storage. For example, a given percent increase in volumetric storage capacity will yield a commensurate percent increase in driving range assuming a fixed-volume tank. In contrast, the same percent increase in gravimetric capacity will yield only a small percent increase in driving range due to the savings in weight of the adsorbent in the fuel tank; therefore, targeting materials based on their total volumetric capacity is a more useful means of identifying candidate materials for H<sub>2</sub> storage. Crystallographic densities are used herein to calculate volumetric capacities as an upper bound of storage capacity, as these represent an intrinsic property of each material and allow for the comparative evaluation of materials across multiple

studies without needing to account for sample preparation or measurement of other densities. The actual storage capacity in a system, however, will depend on the bulk density, shaping, and packing of the storage material, which is outside the scope of this report.<sup>48</sup>

Furthermore, the volumetric usable capacity is the most important consideration when evaluating adsorbents for hydrogen storage. For the purposes of this work, usable capacity is defined as the total amount of H<sub>2</sub> adsorbed between 5 and 100 bar in the total adsorption isotherm (Figure 1). The

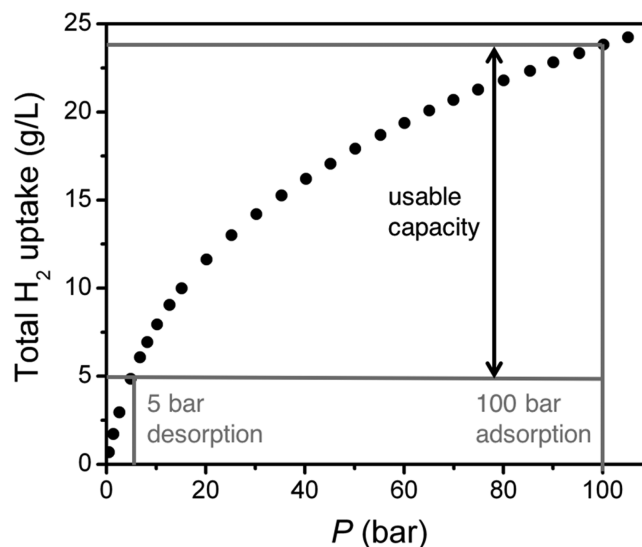


**Figure 1.** An illustration of how usable capacity is calculated, considering adsorption at 100 bar and desorption at 5 bar. For MOFs, usable volumetric capacity is determined from the total uptake and crystallographic density of the material for easy comparison across multiple studies.

total adsorption isotherm is calculated by accounting for the excess capacity plus the amount of bulk H<sub>2</sub> present under the conditions at which the isotherm was measured. The total adsorption thus gives the total amount of gas contained within the volume of a crystal of the adsorbent. A minimum pressure of 5 bar is assumed to be necessary for the fuel injector in the vehicle, such that any H<sub>2</sub> stored below 5 bar is inaccessible as fuel. Thus, all H<sub>2</sub> uptake would ideally occur after 5 bar, and the total capacity would be equal to the usable capacity.<sup>49</sup> In practice, however, materials that strongly bind H<sub>2</sub> typically adsorb large quantities of H<sub>2</sub> at lower pressures, which are then inaccessible to use in the fuel cell.

There are many considerations when measuring adsorption isotherms at high pressures that are crucial for properly evaluating materials for their H<sub>2</sub> adsorption properties. For example, it is important to use a large mass of material to minimize mass errors that may significantly affect the gas uptake. Furthermore, all volumes must be carefully calibrated to ensure reproducibility and accuracy of measurements. Maintaining isothermal control is also essential; regardless of the number of temperature zones in the measurement, consistent volumes at consistent temperatures must be maintained to ensure accuracy across multiple isotherm collections.

The adsorbent cost, which impacts the entire system cost, is another important metric, as the H<sub>2</sub> storage system must be economically competitive with gasoline storage tanks. This

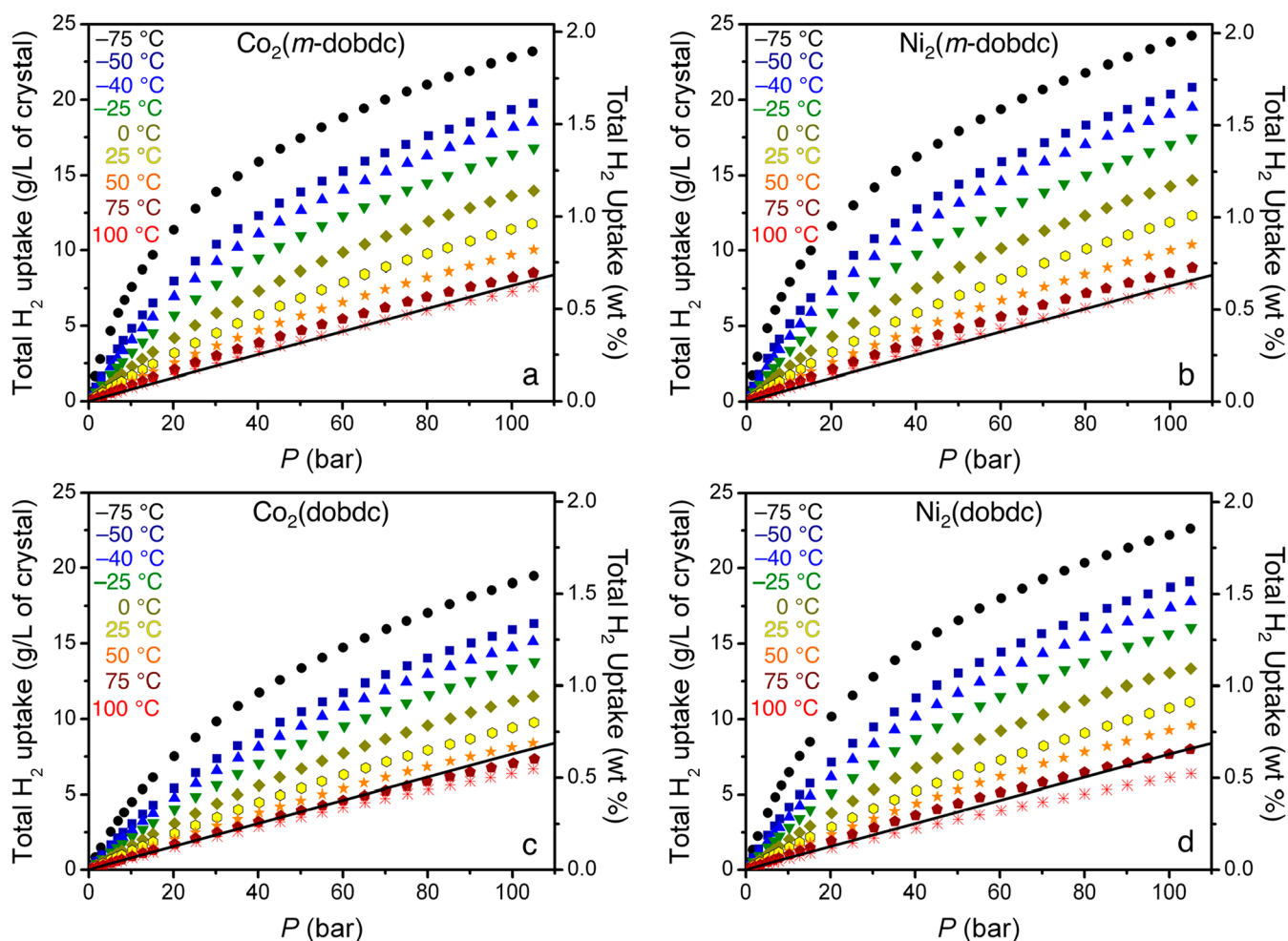


**Figure 2.** Hydrogen adsorption isotherms for (a)  $\text{Co}_2(m\text{-dobdc})$ , (b)  $\text{Ni}_2(m\text{-dobdc})$ , (c)  $\text{Co}_2(\text{dobdc})$ , and (d)  $\text{Ni}_2(\text{dobdc})$  at  $-75$  (black circles),  $-50$  (navy squares),  $-40$  (blue triangles),  $-25$  (green upside-down triangles),  $0$  (gold diamonds),  $25$  (yellow hexagons),  $50$  (orange stars),  $75$  (dark red pentagons), and  $100$  °C (bright red crosses) measured between 0 and 100 bar and plotted in terms of total volumetric and gravimetric capacity. The black line in each plot represents the volumetric density of pure compressed  $\text{H}_2$  at  $25$  °C.

necessity is quite challenging, owing to the relative difficulty of containing a compressed gas versus a liquid fuel. Further, the complexity of synthesis and high precursor expenses for many metal–organic frameworks can render them costly to prepare, limiting their industrial application in gas storage, gas separations, and catalysis. Zeolites currently used in such applications are generally less expensive based on their aluminosilicate composition, although a recent report shows that alternative synthetic routes for MOFs can significantly reduce their cost, making some competitive with zeolites.<sup>50</sup> Furthermore, among MOFs, the  $\text{M}_2(m\text{-dobdc})$  series of materials is particularly poised as a low-cost adsorbent with useful gas adsorption properties. The cost of the  $\text{H}_4(m\text{-dobdc})$  linker is low, as it can be formed in a one-step reaction from cheaply available resorcinol, potassium bicarbonate, and  $\text{CO}_2$ , with no solvent needed other than water during isolation of the product. The overall cost of  $\text{M}_2(m\text{-dobdc})$  itself is thus largely dependent on the metal salt but can be as low as  $\sim \$3/\text{kg}$  for raw materials for the  $\text{Mg}_2(m\text{-dobdc})$  analogue. Such economic considerations are paramount to the successful deployment of MOFs in gas storage applications.

**High-Pressure  $\text{H}_2$  Adsorption Isotherms.** Structural characterization and low-pressure  $\text{H}_2$  adsorption isotherms of  $\text{Co}_2(m\text{-dobdc})$ ,  $\text{Ni}_2(m\text{-dobdc})$ ,  $\text{Co}_2(\text{dobdc})$ ,  $\text{Ni}_2(\text{dobdc})$ , and

MOF-5 have been reported previously.<sup>20,37,39,43</sup> In this study, the high-pressure  $\text{H}_2$  adsorption isotherms of these 5 materials were measured between 0 and 100 bar at temperatures of  $-75$ ,  $-50$ ,  $-40$ ,  $-25$ ,  $0$ ,  $25$ ,  $50$ ,  $75$ , and  $100$  °C. Increments of  $25$  °C were chosen to provide a wide range of conditions for considering temperature swings when determining the volumetric usable capacity of these materials;  $-40$  °C was also measured because it is the temperature at which hydrogen is stored at and dispensed from fueling stations.<sup>51</sup> These isotherms for  $\text{Co}_2(m\text{-dobdc})$ ,  $\text{Ni}_2(m\text{-dobdc})$ ,  $\text{Co}_2(\text{dobdc})$ , and  $\text{Ni}_2(\text{dobdc})$  materials are shown in Figure 2 and for MOF-5 in Figure S1.

Among the five measured materials,  $\text{Ni}_2(m\text{-dobdc})$  exhibits the highest adsorption capacities at all temperatures and pressures, and all isotherms in this material at  $75$  °C and below exhibit a  $\text{H}_2$  capacity higher than that of pure compressed  $\text{H}_2$  at  $25$  °C. At  $25$  °C and 100 bar,  $\text{Ni}_2(m\text{-dobdc})$  takes up 11.9 g of  $\text{H}_2$  per L of crystal, which is the highest among the MOFs measured in this study and, to our knowledge, the highest for any known adsorbent. The usable capacity under these conditions is slightly reduced to 11.0 g/L, however, due to the uptake of 0.9 g/L at 5 bar. This still outperforms compressed hydrogen, which would require compression to over 150 bar to obtain the same total volumetric usable

capacity at 25 °C. At 100 bar and the lowest measured temperature of −75 °C,  $\text{Ni}_2(m\text{-dobdc})$  takes up a total of 23.8 g/L  $\text{H}_2$ , corresponding to a total usable capacity of 19.0 g/L. Notably,  $\text{H}_2$  adsorption data collected at 75.6 K exhibit a total capacity of 57.3 g/L at 105 bar (Figure S2), a value that exceeds the DOE system capacity target, albeit at cryogenic temperatures. Furthermore, data collected at 100 K show capacities at the DOE system capacity targets at 100 bar, which is notable given that measured sample densities were used in calculating the capacity (Figure S3). It is important to note for all of these capacities for  $\text{Ni}_2(m\text{-dobdc})$  and the other materials discussed later that the targets are whole system targets using a material's actual density, while the data presented here is for crystallographic density (except the 100 K isotherm in Figure S3) and simply the material capacity and not the whole system capacity, which is estimated to require 1.2–2 times the target capacities, depending on the material and system design.<sup>52</sup> However, a recent report outlined the synthesis of a high-density HKUST-1 monolith with improved  $\text{CH}_4$  storage capacity relative to that of the bulk material; such a strategy could potentially be applied to  $\text{Ni}_2(m\text{-dobdc})$  as well to retain  $\text{H}_2$  storage capacity in a real system.<sup>53</sup>

If it is possible to use a temperature swing in a storage system through application of active cooling at high filling levels, the usable capacities attained with  $\text{Ni}_2(m\text{-dobdc})$  are even higher. For example, adsorption at −40 °C with desorption at 25 °C affords a usable capacity of 18.2 g/L. An even more extreme temperature swing from adsorption at −75 °C to desorption at 25 °C gives a usable capacity of 23.0 g/L. This enhanced usable capacity represents 77% of the DOE system target of 30 g/L, which is the highest  $\text{H}_2$  volumetric usable capacity achieved to date for an adsorbent operating in this temperature range. It is relevant to note that increasing the desorption temperature to 100 °C offers only an additional 0.4 g/L of usable capacity over desorption at 25 °C, which is not likely to be worthwhile given the additional system complexity required to heat the MOF above ambient temperature.

The related MOFs  $\text{Co}_2(m\text{-dobdc})$ ,  $\text{Co}_2(\text{dobdc})$ , and  $\text{Ni}_2(\text{dobdc})$  were also evaluated for their  $\text{H}_2$  storage performance under various temperature swings, and the results are summarized in Table 2. As the best known adsorbent for

**Table 2. Comparison of the Volumetric Usable Capacities in g/L for Selected Temperature Swings**

	$\text{Co}_2(m\text{-dobdc})$	$\text{Ni}_2(m\text{-dobdc})$	$\text{Co}_2(\text{dobdc})$	$\text{Ni}_2(\text{dobdc})$	MOF-5
25 °C, no swing	10.5	11.0	8.8	9.9	8.8
−75 °C, no swing	18.2	19.0	16.5	18.4	15.8
−40 to 25 °C	17.3	18.2	14.0	16.6	12.8
−75 to 25 °C	21.9	23.0	18.3	21.4	16.5
−75 to 100 °C	22.3	23.4	18.6	21.8	16.7

cryogenic hydrogen storage, MOF-5 was also measured for comparison (Figure S1), and the data agree well with a previous measurement performed at 25 °C.<sup>45</sup> From the results in Table 2,  $\text{Ni}_2(m\text{-dobdc})$  is clearly the top-performing material for all of the considered temperature swings. This superiority arises from it having the highest capacity under all conditions, which is a consequence of the greater charge

density at its open metal coordination sites compared to the other materials. Volumetrically, MOF-5 is inferior to the  $\text{M}_2(m\text{-dobdc})$  and  $\text{M}_2(\text{dobdc})$  adsorbents due to a lack of strong adsorption sites within its pores. While cycling experiments were not completed, we would expect the hydrogen storage capacity to be retained in all of these materials over many cycles, as seen previously in MOF-5.<sup>54</sup>

It is important to understand the benefits that an adsorbent can offer over compression of pure  $\text{H}_2$ . To that end, a comparison of volumetric  $\text{H}_2$  storage capacities at all of the measured temperatures shows that  $\text{Ni}_2(m\text{-dobdc})$  imparts a clear enhancement in capacity relative to the compressed gas (Figure 3). Furthermore, this advantage increases substantially

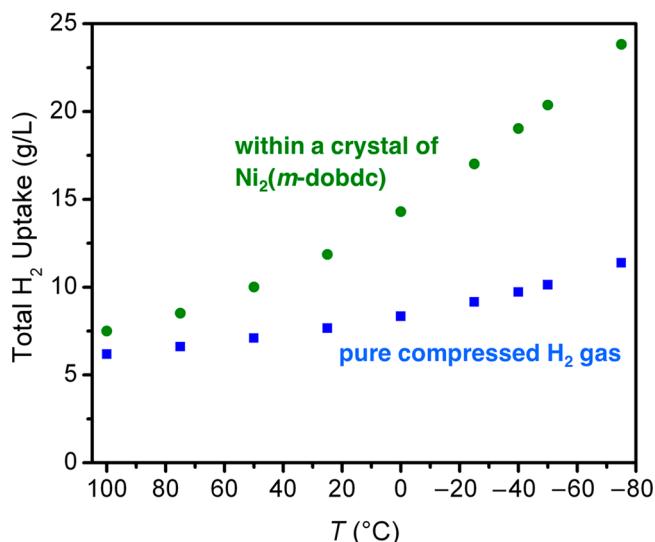


**Figure 3.** Comparison of the total volumetric capacities of  $\text{Ni}_2(m\text{-dobdc})$  (green circles) and pure compressed  $\text{H}_2$  (blue squares), both at 100 bar. Decreasing temperature leads to an increase in the advantage  $\text{Ni}_2(m\text{-dobdc})$  has over pure  $\text{H}_2$  in terms of total volumetric capacity.

with decreasing temperature. Even at 100 °C, the volumetric  $\text{H}_2$  capacity of a crystal of  $\text{Ni}_2(m\text{-dobdc})$  is 121% of the capacity of pure  $\text{H}_2$ . This advantage increases to 155% at 25 °C and 209% at −75 °C, highlighting the utility of  $\text{Ni}_2(m\text{-dobdc})$  for increasing the density of hydrogen in a storage cylinder filled at 100 bar.

**Temperature-Programmed Desorption of  $\text{H}_2$ .** Physisorptive storage of  $\text{H}_2$  (such as in MOFs) has the advantage over chemisorptive storage (such as in metal hydrides) in that the gas is accessible without large energy inputs. As an illustration of this accessibility and the stronger binding in the  $\text{M}_2(m\text{-dobdc})$  series, we carried out temperature-programmed desorption (TPD) experiments on samples of  $\text{Ni}_2(m\text{-dobdc})$  and  $\text{Ni}_2(\text{dobdc})$  loaded with  $\text{H}_2$ .

The results of the TPD measurements indicate that  $\text{Ni}_2(m\text{-dobdc})$  binds  $\text{H}_2$  more strongly, given the shift in the desorption profile of  $\text{H}_2$  as compared with  $\text{Ni}_2(\text{dobdc})$  (Figure 4). These desorption peaks, centered at −165 and −175 °C for  $\text{Ni}_2(m\text{-dobdc})$  and  $\text{Ni}_2(\text{dobdc})$ , respectively, appear to indicate that both materials polarize  $\text{H}_2$  strongly enough that it desorbs above liquid nitrogen temperature (−198 °C at the NREL altitude). Empirical differences in desorption temperature between materials typically arise due to differences in pore shape or size, which impact the diffusion of hydrogen through



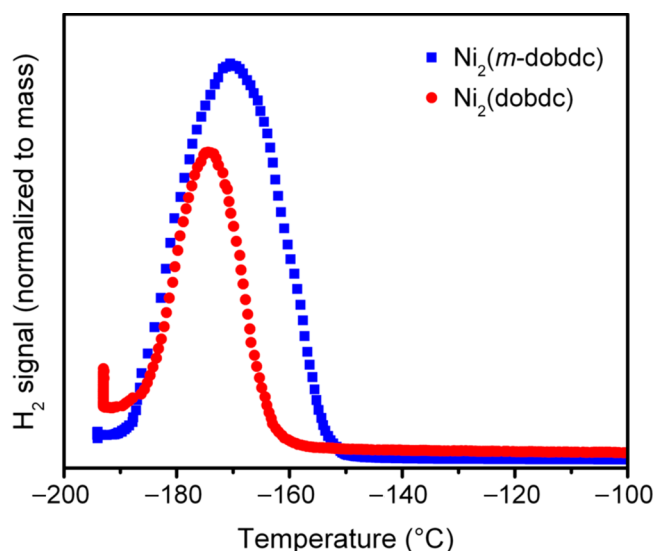


**Figure 4.** Temperature-programmed desorption of  $\text{H}_2$  in  $\text{Ni}_2(m\text{-dobdc})$  and  $\text{Ni}_2(\text{dobdc})$ . Note the difference in desorption temperature between  $\text{Ni}_2(m\text{-dobdc})$  and  $\text{Ni}_2(\text{dobdc})$ .

the pores. However, due to the similar pore shapes and sizes exhibited by these two MOFs, the higher desorption temperature for  $\text{Ni}_2(m\text{-dobdc})$  is indicative of a stronger  $\text{H}_2$  binding at the open  $\text{Ni}^{2+}$  sites.

**In Situ Powder Neutron Diffraction.** Powder neutron diffraction experiments were undertaken at high pressures to further understand hydrogen adsorption in the  $\text{M}_2(m\text{-dobdc})$  frameworks. The measurements were performed on  $\text{Co}_2(m\text{-dobdc})$ , as its greater degree of crystallinity allowed for structure solutions of the  $\text{D}_2$ -dosed samples and the refinement of the  $\text{D}_2$  adsorption positions within the pores. While not a direct measure of the performance of  $\text{Ni}_2(m\text{-dobdc})$ , the similar structure and adsorption behavior of  $\text{Co}_2(m\text{-dobdc})$  should provide a representative example of the  $\text{Ni}_2(m\text{-dobdc})$  material. Additionally,  $\text{D}_2$  and  $\text{H}_2$  have previously been shown to behave nearly identically in powder neutron diffraction experiments.<sup>39</sup> Samples were measured at 198 K at pressures of 36, 54, and 79 bar, as well as at 77 K at a pressure of 78 bar to most closely simulate the adsorption isotherm conditions while retaining the ability to crystallographically locate each  $\text{D}_2$  binding site within the pores.

At 77 K, the sample of  $\text{Co}_2(m\text{-dobdc})$  loaded with  $\text{D}_2$  at 78 bar revealed 7 distinct adsorption sites (Figure 5). At site 1, the strongest adsorption site, the  $\text{D}_2$  is bound to the open  $\text{Co}^{2+}$  coordination site with a  $\text{Co}\cdots\text{D}_2(\text{centroid})$  separation of 2.25(7) Å. The  $\text{D}_2$  at site 2 is directly adjacent, interacting with both the  $\text{D}_2$  bound at site 1 as well as ligand O atoms from a hydroxide and a carboxylate. Site 3 occupies a position above the center of the aromatic ring of the  $m\text{-dobdc}^{4-}$  linker, while site 4 lies adjacent to this. These first four adsorption sites were previously observed in neutron diffraction experiments carried out on  $\text{Co}_2(m\text{-dobdc})$  at 4 K and pressures below 1 bar.<sup>39</sup> Adsorption sites 5–7, which become occupied only at the higher  $\text{D}_2$  pressures measured here, could likely have been located in the previous study if higher dosings were used. Sites 5 and 6 lie at the center of the hexagonal channels of the framework, while site 7 resides 3.10(3) Å from the  $\text{D}_2$  located at site 5 and primarily relies on  $\text{D}_2\cdots\text{D}_2$  interactions for stabilization. At 77 K and 78 bar, sites 1–6 show full occupancy of  $\text{D}_2$ , and site 7 shows approximately half

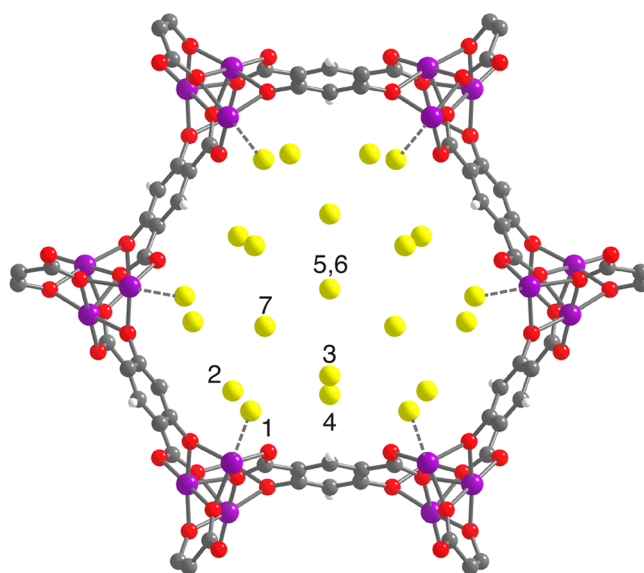


**Figure 5.** A single pore of  $\text{Co}_2(m\text{-dobdc})$  showing the seven distinct  $\text{D}_2$  binding sites as determined from neutron diffraction data. Purple, red, gray, white, and yellow spheres represent Co, O, C, and H atoms and  $\text{D}_2$  molecules, respectively.

occupancy. Importantly, a comparison of the adsorption isotherm data collected at 198 K and the  $\text{D}_2$  loadings observed by powder neutron diffraction at the same temperature reveal a quantitative agreement between the two methods for measuring storage capacity (Figure S4).

Notably, the  $\text{D}_2\cdots\text{D}_2$  distances (Table 3) measured for certain sites within the pores of  $\text{Co}_2(m\text{-dobdc})$  are very short.

**Table 3. Selected  $\text{D}_2\cdots\text{D}_2$  Distances within  $\text{Co}_2(m\text{-dobdc})$  as Determined from Powder Neutron Diffraction Collected at 77 K and 78 bar<sup>a</sup>**

$\text{D}_2\cdots\text{D}_2$ interaction	distance (Å)
1...2	2.86(3)
2...2	3.08(3)
3...4	3.12(5)
4...5	3.41(3)
solid $\text{H}_2$ <sup>55</sup>	3.21

<sup>a</sup>Numbers in parentheses indicate one standard deviation in the value.

For example, the distance between the  $\text{D}_2$  molecules at sites 1 and 2 is only 2.86(3) Å. This is significantly shorter than the  $\text{H}_2\cdots\text{H}_2$  separation of 3.21 Å in solid hydrogen,<sup>55</sup> and is approaching the  $\text{H}_2\cdots\text{H}_2$  distance of 2.656 Å in solid  $\text{H}_2$  pressurized to 54 kbar at 300 K.<sup>56</sup> These comparisons to solid hydrogen powerfully illustrate the ability of materials in the  $\text{M}_2(m\text{-dobdc})$  series to densify hydrogen within their pores. Other notably short  $\text{D}_2\cdots\text{D}_2$  distances within  $\text{Co}_2(m\text{-dobdc})$  can be seen in Table 3, further illustrating this principle.<sup>57</sup> Significantly, the high charge density on the metals not only strongly polarizes  $\text{D}_2$  bound at the coordinatively unsaturated  $\text{Co}^{2+}$  center, but additionally impacts  $\text{D}_2$  bound in more weakly physisorbing secondary sites as well, leading to a high hydrogen packing density within the adsorbent.

**In Situ Infrared Spectroscopy.** High-pressure  $\text{H}_2$ -dosed *in situ* infrared spectroscopy was used to further understand  $\text{H}_2$  loading in  $\text{Ni}_2(m\text{-dobdc})$ . Spectra were collected in the pressure range 10–90 bar at multiple temperatures ranging

from 198 K (Figure 6) to 298 K (Figures S11–S19). Adsorbed  $\text{H}_2$  in MOFs has been shown to exhibit a vibrational frequency

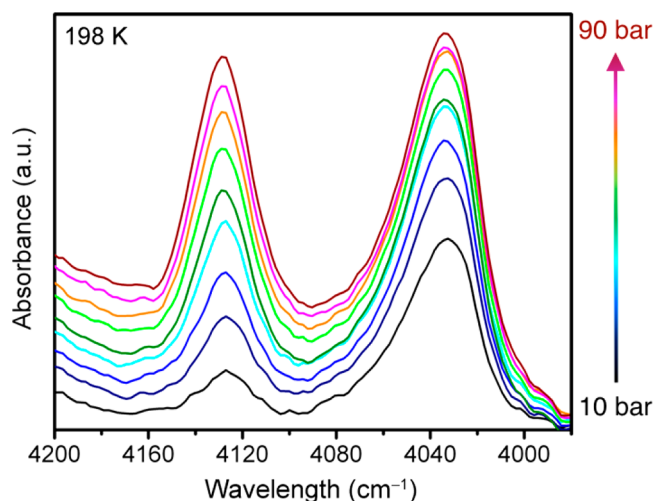


**Figure 6.** *In situ*  $\text{H}_2$ -dosed infrared spectroscopy of  $\text{Ni}_2(m\text{-dobdc})$  at 198 K with  $\text{H}_2$  pressure between 10 and 90 bar. Note that the spectra have been offset for clarity. The peak on the right corresponds to  $\text{H}_2$  bound to the open  $\text{Ni}^{2+}$  site, and the peak on the left corresponds to  $\text{H}_2$  bound at secondary sites within the pores.

that is lower than that of free gaseous  $\text{H}_2$  ( $4161\text{ cm}^{-1}$ ) and generally correlates with the  $\text{H}_2$  binding energy at a given site.<sup>58</sup> In Figure 6, the peak at  $\sim 4035\text{ cm}^{-1}$  corresponds to  $\text{H}_2$  bound to the open  $\text{Ni}^{2+}$  sites in the framework, while the peak at  $\sim 4125\text{ cm}^{-1}$  corresponds to  $\text{H}_2$  adsorbed at more weakly interacting secondary sites within the pores. At lower pressures, the peak area of the  $\text{Ni}^{2+}$ -bound  $\text{H}_2$  is significantly larger than that of the peak area at the secondary sites, indicating a substantially higher  $\text{H}_2$  binding enthalpy.

As the gas pressure is increased, the area of the secondary site peak grows with the corresponding increase in adsorbed  $\text{H}_2$  within the pores. A commensurate increase is not seen for the  $\text{Ni}^{2+}$ -bound  $\text{H}_2$ , as saturation of these sites prior to the occupation of secondary sites is likely. A comparison of the peak areas calculated from these spectra, which should be proportional to the  $\text{H}_2$  loading, shows good agreement with the isotherm data when a single linear scaling factor (used to compare absolute adsorption from isotherms to the relative adsorption determined by infrared spectroscopy) is applied to the peaks areas at each temperature (Figures S11–S19), especially at pressures below 60 bar. The small standard deviations for the observed scaling factors ( $<0.8$  for all temperatures and  $<0.3$  for 198 and 233 K) support the validity of this method (Table S6).

Figure 7 displays infrared spectra collected for  $\text{Ni}_2(m\text{-dobdc})$  at approximately equivalent  $\text{H}_2$  loadings at various temperatures and pressures. The results illustrate how the loading of each of the two types of adsorption sites ( $\text{Ni}^{2+}$  centers at  $4035\text{ cm}^{-1}$  and more weakly physisorbing sites at  $4125\text{ cm}^{-1}$ ) changes as a function of temperature. At 273 K and 70 bar, the area under the peaks for each binding site are approximately equal, indicating an even distribution of bound  $\text{H}_2$  between the open  $\text{Ni}^{2+}$  sites and other sites within the pores. As the temperature is decreased, the pressure drops as more  $\text{H}_2$  adsorbs in the material, and the peak at  $4035\text{ cm}^{-1}$  begins to grow while the peak at  $4125\text{ cm}^{-1}$  shrinks, indicating a shift toward more adsorption at the open  $\text{Ni}^{2+}$  sites. At 198 K

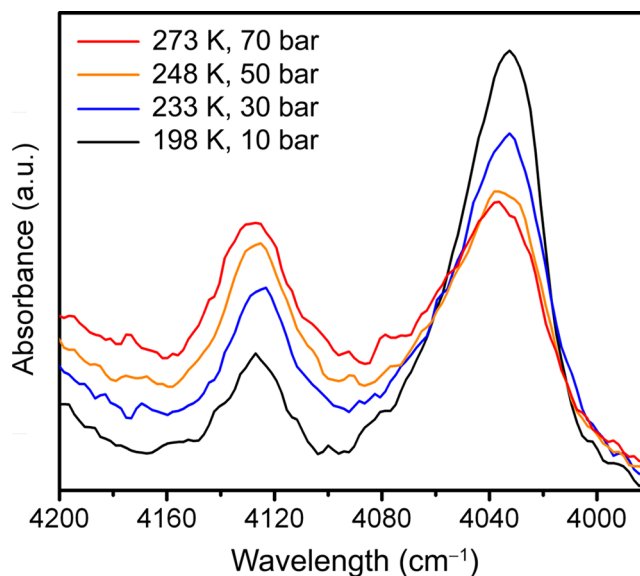


**Figure 7.** Comparison of infrared spectra with approximately constant adsorption of  $\text{H}_2$  in  $\text{Ni}_2(m\text{-dobdc})$  based on total peak area for each spectrum. Note the change in relative peak areas from approximately equal loading of open  $\text{Ni}^{2+}$  sites ( $\sim 4035\text{ cm}^{-1}$ ) and other sites ( $\sim 4125\text{ cm}^{-1}$ ) at 273 K and 70 bar to a much higher concentration of  $\text{H}_2$  bound to the open  $\text{Ni}^{2+}$  sites at 198 K and 10 bar.

and 10 bar, most of the adsorbed  $\text{H}_2$  is bound to the open metal sites. This confirmation of the temperature dependence of the binding site population, while expected, is quite interesting and illustrates the importance of operating conditions when considering the use of an adsorbent in a hydrogen storage system.

## CONCLUSIONS

Selected high-performance metal–organic frameworks were evaluated for their  $\text{H}_2$  adsorption properties under conditions relevant to on-board storage in motor vehicles. Adsorption isotherms in the pressure range of 0–100 bar were measured for the materials  $\text{Co}_2(m\text{-dobdc})$ ,  $\text{Ni}_2(m\text{-dobdc})$ ,  $\text{Co}_2(\text{dobdc})$ , and  $\text{Ni}_2(\text{dobdc})$ , which contain a high density of coordinatively unsaturated metal sites, as well as for MOF-5, which does not.  $\text{Ni}_2(m\text{-dobdc})$  is the top-performing material with respect to the critical metric of usable volumetric  $\text{H}_2$  capacity at pressures between 5 and 100 bar and near-ambient temperatures. To our knowledge, this compound displays the highest physisorptive hydrogen storage capacity of any known adsorbent under these conditions. Its high capacity is attributable to the presence of highly polarizing  $\text{Ni}^{2+}$  adsorption sites, which lead to large binding enthalpies and a dense packing of  $\text{H}_2$  within the material. This conclusion is supported by the results of temperature-programmed desorption, *in situ* powder neutron diffraction, and *in situ* infrared spectroscopy experiments performed under relevant conditions. The results provide benchmark data for comparison with future generations of adsorbents designed for hydrogen storage. In particular, efforts are underway to create new metal–organic frameworks with low-coordinate metal cations capable of binding multiple  $\text{H}_2$  molecules at enthalpies in the optimal range of  $-15$  to  $-20\text{ kJ/mol}$ . Lastly, this study highlights the importance of adsorption conditions in the evaluation of materials and the superior performance of



metal–organic frameworks containing open metal coordination sites for physisorptive H<sub>2</sub> storage.

## ■ ASSOCIATED CONTENT

### ■ Supporting Information

The Supporting Information is available free of charge on the ACS Publications website at DOI: 10.1021/acs.chemmater.8b03276.

Additional experimental data, H<sub>2</sub> adsorption isotherms, powder neutron diffraction structures, H<sub>2</sub>-dosed infrared spectroscopy data, and other data (PDF)

Crystallographic information files (ZIP)

## ■ AUTHOR INFORMATION

### Corresponding Author

\*E-mail: jrlong@berkeley.edu.

### ORCID

Stephen A. FitzGerald: 0000-0001-9492-9256

Jeffrey R. Long: 0000-0002-5324-1321

### Author Contributions

M.T.K. and J.R.L. formulated the project. M.T.K. synthesized the compounds. M.T.K., K.E.H., P.A.P., and T.G. collected and analyzed isotherm data. K.E.H. and T.G. collected temperature-programmed desorption data. T.R., J.D.T., A.A., and C.M.B. collected powder neutron diffraction data and solved crystal structures. T.R., H.Z.H.J., and S.A.F. collected and analyzed infrared spectra. M.T.K. and J.R.L. wrote the paper, and all authors contributed to revising it. All authors have given approval to the final version of the manuscript.

### Notes

The authors declare the following competing financial interest(s): J.R.L. has a financial interest in Mosaic Materials, Inc., a startup company working to commercialize metal–organic frameworks, including the M2(m-dobdc) materials. The University of California, Berkeley has applied for a patent on some of the materials discussed herein, on which J.R.L. and M.T.K. are listed as inventors.

## ■ ACKNOWLEDGMENTS

This work was fully supported by the United States Department of Energy (USDOE), Office of Energy Efficiency and Renewable Energy (EERE), Fuel Cell Technologies Office (FCTO), under Contract DE-AC02-05CH11231. We thank the NSF for providing graduate fellowship support for M.T.K., the US Department of Energy, Office of Energy Efficiency and Renewable Energy, Fuel Cell Technologies Office, for support of J.D.T. under Contract DE-AC36-08GO28308, and the NSF for support of S.A.F. through Grant CHE-1111896. We also thank Rodolfo Torres-Gavosto for the improved H<sub>2</sub>(m-dobdc) synthesis; Q. Barker-Plummer, D. Mukasa, J. Parker, and E. Rapoport for experimental assistance; and Dr. Katie R. Meihaus for editorial assistance. Certain commercial equipment, instruments, or materials are identified in this document. Such identification does not imply recommendation or endorsement by the National Institute of Standards and Technology nor does it imply that the products identified are necessarily the best available for the purpose. The views and opinions of the authors expressed herein do not necessarily state or reflect those of the United States Government or any agency thereof. Neither the United States Government nor any agency thereof, nor any of their employees, makes any

warranty, expressed or implied, or assumes any legal liability or responsibility for the accuracy, completeness, or usefulness of any information, apparatus, product, or process disclosed, or represents that its use would not infringe privately owned rights.

## ■ REFERENCES

- (1) Hoffmann, P. *Tomorrow's Energy: Hydrogen, Fuel Cells, and the Prospects for a Cleaner Planet*; The MIT Press: Cambridge, MA, 2012.
- (2) Alternative Fuels Data Center. [http://www.afdc.energy.gov/fuels/hydrogen\\_locations.html](http://www.afdc.energy.gov/fuels/hydrogen_locations.html) (accessed April 23, 2017).
- (3) AB-8 Alternative Fuel and Vehicle Technologies: Funding Programs. [http://leginfo.ca.gov/faces/billNavClient.xhtml?bill\\_id=201320140AB8](http://leginfo.ca.gov/faces/billNavClient.xhtml?bill_id=201320140AB8) (accessed April 25, 2017).
- (4) Fuel Cell Technologies Market Report 2015. [https://energy.gov/sites/prod/files/2016/10/f33/fcto\\_2015\\_market\\_report.pdf](https://energy.gov/sites/prod/files/2016/10/f33/fcto_2015_market_report.pdf) (accessed April 25, 2017).
- (5) H2USA. <http://www.h2usa.org/> (accessed April 25, 2017). International Partnership for Hydrogen and Fuel Cells in the Economy. <http://www.iphe.net/> (accessed April 25, 2017). California Fuel Cell Partnership. <http://cafcp.org/> (accessed April 25, 2017). Low Carbon Vehicle Partnership. <http://www.lowcvp.org.uk/> (accessed April 25, 2017). U.S. Drive Partnership. [https://www.hydrogen.energy.gov/usdrive\\_partnership.html](https://www.hydrogen.energy.gov/usdrive_partnership.html) (accessed April 25, 2017). Scandinavian Hydrogen Highway Partnership. <http://www.scandinavianhydrogen.org/shhp/vehicles/> (accessed April 25, 2017).
- (6) Schlapbach, L.; Züttel, A. Hydrogen-storage materials for mobile applications. *Nature* **2001**, 414, 353–358.
- (7) Midilli, A.; Ay, M.; Dincer, I.; Rosen, M. A. On hydrogen and hydrogen energy strategies: I: current status and needs. *Renewable Sustainable Energy Rev.* **2005**, 9, 255–271.
- (8) Mazloomi, K.; Gomes, C. Hydrogen as an energy carrier: prospects and challenges. *Renewable Sustainable Energy Rev.* **2012**, 16, 3024–3033.
- (9) Arnold, G.; Eberle, U.; Hasenauer, D. Apparatus for optimal adsorption and desorption of gases utilizing highly porous gas storage materials. *US Patent* US7517396 B2, 2009.
- (10) Züttel, A. Materials for hydrogen storage. *Mater. Today* **2003**, 6, 24–33.
- (11) H35 (35 MPa/350 bar) vs. H70 (70 MPa/700 bar) Fueling Mirai Refueling Tips. [https://ssl.toyota.com/mirai/Mirai\\_Fueling.pdf](https://ssl.toyota.com/mirai/Mirai_Fueling.pdf) (accessed January 15, 2017).
- (12) Jepsen, L. H.; Ley, M. B.; Lee, Y.-S.; Cho, Y. W.; Dornheim, M.; Jensen, J. O.; Filinchuk, Y.; Jørgensen, J. E.; Besenbacher, F.; Jensen, T. R. Boron-nitrogen based hydrides and reactive composites for hydrogen storage. *Mater. Today* **2014**, 17, 129–135.
- (13) Zhu, Q.-L.; Xu, Q. Liquid organic and inorganic chemical hydrides for high-capacity hydrogen storage. *Energy Environ. Sci.* **2015**, 8, 478–512.
- (14) He, T.; Pachfule, P.; Wu, H.; Xu, Q.; Chen, P. Hydrogen carriers. *Nat. Rev. Mater.* **2016**, 1, 16059.
- (15) Rusman, N. A. A.; Dahari, M. A review on the current progress of metal hydrides material for solid-state hydrogen storage applications. *Int. J. Hydrogen Energy* **2016**, 41, 12108–12126.
- (16) Dündar-Tekkaya, E.; Yürüm, Y. Mesoporous MCM-41 material for hydrogen storage: A short review. *Int. J. Hydrogen Energy* **2016**, 41, 9789–9795.
- (17) Blankenship, T. S.; Mokaya, R. Cigarette butt-derived carbons have ultra-high surface area and unprecedented hydrogen capacity. *Energy Environ. Sci.* **2017**, 10, 2552–2562.
- (18) Ahluwalia, R. K.; Peng, J. K. Automotive hydrogen storage system using cryo-adsorption on activated carbon. *Int. J. Hydrogen Energy* **2009**, 34, 5476–5487.
- (19) Petitpas, G.; Bénard, P.; Klebanoff, L. E.; Xiao, J.; Aceves, S. A comparative analysis of the cryo-compression and cryo-adsorption hydrogen storage methods. *Int. J. Hydrogen Energy* **2014**, 39, 10564–10584.

- (20) Rosi, N. L.; Eckert, J.; Eddaoudi, M.; Vodak, D. T.; Kim, J.; O'Keeffe, M.; Yaghi, O. M. Hydrogen Storage in Microporous Metal-Organic Frameworks. *Science* **2003**, *300*, 1127.
- (21) Farha, O. K.; Eryazici, I.; Jeong, N. C.; Hauser, B. G.; Wilmer, C. E.; Sarjeant, A. A.; Snurr, R. Q.; Nguyen, S. T.; Yazaydin, A. O.; Hupp, J. T. Metal-Organic Framework Materials with Ultrahigh Surface Areas: Is the Sky the Limit? *J. Am. Chem. Soc.* **2012**, *134*, 15016–15021.
- (22) Krause, S.; Bon, V.; Senkovska, I.; Stoeck, U.; Wallacher, D.; Többs, D. M.; Zander, S.; Pillai, R. S.; Maurin, G.; Coudert, F.-X.; Kaskel, S. A pressure-amplifying framework material with negative gas adsorption transitions. *Nature* **2016**, *532*, 348–352.
- (23) Yuan, S.; Chen, Y.-P.; Qin, J.-S.; Lu, W.; Zou, L.; Zhang, Q.; Wang, X.; Sun, X.; Zhou, H.-C. Linker Installation: Engineering Pore Environment with Precisely Placed Functionalities in Zirconium MOFs. *J. Am. Chem. Soc.* **2016**, *138*, 8912–8919.
- (24) Murray, L. J.; Dincă, M.; Long, J. R. Hydrogen storage in metal-organic frameworks. *Chem. Soc. Rev.* **2009**, *38*, 1294–1314.
- (25) Suh, M. P.; Park, H. J.; Prasad, T. K.; Lim, D.-W. Hydrogen Storage in Metal-Organic Frameworks. *Chem. Rev.* **2012**, *112*, 782–835.
- (26) Basdogan, Y.; Keskin, S. Simulation and modelling of MOFs for hydrogen storage. *CrystEngComm* **2015**, *17*, 261–275.
- (27) Gómez-Gualdrón, D. A.; Colón, Y. J.; Zhang, X.; Wang, T. C.; Chen, Y.-S.; Hupp, J. T.; Yildirim, T.; Farha, O. K.; Zhang, J.; Snurr, R. Q. Evaluating topologically diverse metal-organic frameworks for cry-adsorbed hydrogen storage. *Energy Environ. Sci.* **2016**, *9*, 3279–3289.
- (28) Rahali, S.; Belhocine, Y.; Seydou, M.; Maurel, F.; Tangour, B. Multiscale study of the structure and hydrogen storage capacity of an aluminium metal-organic framework. *Int. J. Hydrogen Energy* **2017**, *42*, 15271–15282.
- (29) Han, S. S.; Goddard, W. A., III Lithium-Doped Metal-Organic Frameworks for Reversible H<sub>2</sub> Storage at Ambient Temperature. *J. Am. Chem. Soc.* **2007**, *129*, 8422–8423.
- (30) Rao, D.; Lu, R.; Xiao, C.; Kan, E.; Deng, K. Lithium-doped MOF impregnated with lithium-coated fullerenes: A hydrogen storage route for high gravimetric and volumetric uptakes at ambient temperatures. *Chem. Commun.* **2011**, *47*, 7698–7700.
- (31) Meng, Z.; Lu, R.; Rao, D.; Kan, E.; Xiao, C.; Deng, K. Catenated metal-organic frameworks: Promising hydrogen purification materials and high hydrogen storage medium with further lithium doping. *Int. J. Hydrogen Energy* **2013**, *38*, 9811–9818.
- (32) Bhatia, S. K.; Myers, A. L. Optimum Conditions for Adsorptive Storage. *Langmuir* **2006**, *22*, 1688–1700.
- (33) DOE. Technical Targets for Onboard Hydrogen Storage for Light-Duty Vehicles, <https://energy.gov/eere/fuelcells/doe-technical-targets-onboard-hydrogen-storage-light-duty-vehicles> (accessed April 25, 2017).
- (34) Dincă, M.; Long, J. R. Hydrogen Storage in Microporous Metal-Organic Frameworks with Exposed Metal Sites. *Angew. Chem., Int. Ed.* **2008**, *47*, 6766–6779.
- (35) Dincă, M.; Dailly, A.; Liu, Y.; Brown, C. M.; Neumann, D. A.; Long, J. R. Hydrogen Storage in a Microporous Metal-Organic Framework with Exposed Mn<sup>2+</sup> Coordination Sites. *J. Am. Chem. Soc.* **2006**, *128*, 16876–16883.
- (36) Vitillo, J. G.; Regli, L.; Chavan, S.; Ricchiardi, G.; Spoto, G.; Dietzel, P. D. C.; Bordiga, S.; Zecchina, A. Role of Exposed Metal Sites in Hydrogen Storage in MOFs. *J. Am. Chem. Soc.* **2008**, *130*, 8386–8396.
- (37) Zhou, W.; Wu, H.; Yildirim, T. Enhanced H<sub>2</sub> Adsorption in Isostructural Metal-Organic Frameworks with Open Metal Sites: Strong Dependence of the Binding Strength on Metal Ions. *J. Am. Chem. Soc.* **2008**, *130*, 15268–15269.
- (38) Oh, H.; Savchenko, I.; Mavrandonakis, A.; Heine, T.; Hirscher, M. Highly Effective Hydrogen Isotope Separations in Nanoporous Metal-Organic Frameworks with Open Metal Sites: Direct Measurement and Theoretical Analysis. *ACS Nano* **2014**, *8*, 761–770.
- (39) Kapelewski, M. T.; Geier, S. J.; Hudson, M. R.; Stück, D.; Mason, J. A.; Nelson, J. N.; Xiao, D. J.; Hulvey, Z.; Gilmour, E.; FitzGerald, S. A.; Head-Gordon, M.; Brown, C. M.; Long, J. R. M<sub>2</sub>(m-dobdc) (M = Mg, Mn, Fe, Co, Ni) Metal-Organic Frameworks Exhibiting Increased Charge Density and Enhanced H<sub>2</sub> Binding at the Open Metal Sites. *J. Am. Chem. Soc.* **2014**, *136*, 12119–12129.
- (40) Denysenko, D.; Grzywa, M.; Jelic, J.; Reuter, K.; Volkmer, D. Scorpionate-Type Coordination in MFU-4l Metal-Organic Frameworks: Small-Molecule Binding and Activation upon the Thermally Activated Formation of Open Metal Sites. *Angew. Chem., Int. Ed.* **2014**, *53*, 5832–5836.
- (41) Weinrauch, I.; Savchenko, I.; Denysenko, D.; Souliou, S. M.; Kim, H.-H.; Le Tacon, M.; Daemen, L. L.; Cheng, Y.; Mavrandonakis, A.; Ramirez-Cuesta, A. J.; Volkmer, D.; Schütz, G.; Hirscher, M.; Heine, T. Capture of heavy hydrogen isotopes in a metal-organic framework with active Cu(I) sites. *Nat. Commun.* **2017**, *8*, 14496.
- (42) Mason, J. A.; Veenstra, M.; Long, J. R. Evaluating metal-organic frameworks for natural gas storage. *Chem. Sci.* **2014**, *5*, 32–51.
- (43) Kaye, S. S.; Dailly, A.; Yaghi, O. M.; Long, J. R. Impact of Preparation and Handling on the Hydrogen Storage Properties of Zn<sub>4</sub>O(1,4-benzenedicarboxylate)<sub>3</sub> (MOF-5). *J. Am. Chem. Soc.* **2007**, *129*, 14176–14177.
- (44) Hurst, K. E.; Heben, M. J.; Blackburn, J. L.; Gennett, T.; Dillon, A. C.; Parilla, P. A. A dynamic calibration technique for temperature programmed desorption spectroscopy. *Rev. Sci. Instrum.* **2013**, *84*, 025103.
- (45) FitzGerald, S. A.; Churchill, H. O. H.; Korngut, P. M.; Simmons, C. B.; Strangas, Y. E. Cryogenic apparatus for diffuse reflection infrared spectroscopy with high-pressure capabilities. *Rev. Sci. Instrum.* **2006**, *77*, 093110.
- (46) Goldsmith, J.; Wong-Foy, A. G.; Cafarella, M. J.; Siegel, D. J. Theoretical Limits of Hydrogen Storage in Metal-Organic Frameworks: Opportunities and Trade-Offs. *Chem. Mater.* **2013**, *25*, 3373–3382.
- (47) Gómez-Gualdrón, D. A.; Wang, T. C.; García-Holley, P.; Sawelewa, R. M.; Argueta, E.; Snurr, R. Q.; Hupp, J. T.; Yildirim, T.; Farha, O. K. Understanding Volumetric and Gravimetric Hydrogen Adsorption Trade-off in Metal-Organic Frameworks. *ACS Appl. Mater. Interfaces* **2017**, *9*, 33419–33428.
- (48) Parilla, P. A.; O'Neil, K. J.; Hurst, K.; Gennett, T. An international multi-laboratory investigation of carbon-based hydrogen sorbent materials. *Appl. Phys. A: Mater. Sci. Process.* **2016**, *122*, 42.
- (49) Mason, J. A.; Oktawiec, J.; Taylor, M. K.; Hudson, M. R.; Rodriguez, J.; Bachman, J. E.; Gonzalez, M. I.; Cervellino, A.; Guagliardi, A.; Brown, C. M.; Llewellyn, P. L.; Masciocchi, N.; Long, J. R. Methane storage in flexible metal-organic frameworks with intrinsic thermal management. *Nature* **2015**, *527*, 357–361.
- (50) DeSantis, D.; Mason, J. A.; James, B. D.; Houchins, C.; Long, J. R.; Veenstra, M. Techno-Economic Analysis of Metal-Organic Frameworks for Hydrogen and Natural Gas Storage. *Energy Fuels* **2017**, *31*, 2024–2032.
- (51) Parks, G.; Boyd, R.; Cornish, J.; Remick, R.; Popovich, N. *Hydrogen Station Compression, Storage, and Dispensing Technical Status and Costs*; NREL: Golden, CO, 2014 <http://www.nrel.gov/docs/fy14osti/58564.pdf>.
- (52) Satyapal, S.; Petrovic, J.; Read, C.; Thomas, G.; Ordaz, G. The U.S. Department of Energy's National Hydrogen Storage Project: Progress towards meeting hydrogen-powered vehicle requirements. *Catal. Today* **2007**, *120*, 246–256.
- (53) Tian, T.; Zeng, Z.; Vulpe, D.; Casco, M. E.; Divitini, G.; Midgley, P. A.; Silvestre-Albero, J.; Tan, J.-C.; Moghadam, P. Z.; Fairen-Jimenez, D. A sol-gel monolithic metal-organic frameworks with enhanced methane uptake. *Nat. Mater.* **2017**, *17*, 174–179.
- (54) Ming, Y.; Purewal, J.; Yang, J.; Xu, C.; Veenstra, M.; Gaab, M.; Müller, U.; Siegel, D. J. Stability of MOF-5 in a hydrogen gas environment containing fueling station impurities. *Int. J. Hydrogen Energy* **2016**, *41*, 9374–9382.
- (55) van Kranendonk, J.; Gush, H. P. The crystal structure of solid hydrogen. *Phys. Lett.* **1962**, *1*, 22–23.

(56) Mao, H. K.; Jephcoat, A. P.; Hemley, R. J.; Finger, L. W.; Zha, C. S.; Hazen, R. M.; Cox, D. E. Synchrotron X-ray Diffraction Measurements of Single-Crystal Hydrogen to 26.5 Gigapascals. *Science* **1988**, 239, 1131–1134.

(57) Liu, Y.; Kabbour, H.; Brown, C. M.; Neumann, D. A.; Ahn, C. C. Increasing the Density of Adsorbed Hydrogen with Coordinatively Unsaturated Metal Centers in Metal-Organic Frameworks. *Langmuir* **2008**, 24, 4772–4777.

(58) FitzGerald, S. A.; Burkholder, B.; Friedman, M.; Hopkins, J. B.; Pierce, C. J.; Schloss, J. M.; Thompson, B.; Rowsell, J. L. C. Metal-Specific Interactions of H<sub>2</sub> Adsorbed within Isostructural Metal-Organic Frameworks. *J. Am. Chem. Soc.* **2011**, 133, 20310–20318.